Journal of Alloys and Compounds 854 (2021) 157275

Contents lists available at ScienceDirect

Journal of Alloys and Compounds

journal homepage: http://www.elsevier.com/locate/jalcom

Hot deformation behavior and microstructure evolution of carbon nanotube/7055Al composite

K. Ma [a, b], Z.Y. Liu [a, *], X.X. Zhang [a], B.L. Xiao [a, **], Z.Y. Ma [a, c]

[a] Shi-changxu Innovation Center for Advanced Materials, Institute of Metal Research, Chinese Academy of Science, 72 Wenhua Road, Shenyang, 110016, China
[b] School of Materials Science and Engineering, University of Science and Technology of China, 72 Wenhua Road, Shenyang, 110016, China
[c] Key Laboratory of New Processing Technology for Nonferrous Metal & Materials, Ministry of Education, Guilin University of Technology, Guilin, 541004, China

ARTICLE INFO

Article history:
Received 20 February 2020
Received in revised form
17 September 2020
Accepted 18 September 2020
Available online 21 September 2020

Keywords:
Carbon nanotube
Aluminum matrix composite
Hot deformation
Abnormal grain growth

ABSTRACT

In this study, carbon nanotube (CNT) reinforced 7055Al composite was fabricated by high energy ball milling combined with powder metallurgy. The as hot-pressed composite had an inhomogeneous microstructure composed of coarse grains without CNTs and fine grains with uniformly dispersed CNTs. Processing maps were established and the hot deformation behavior as well as the microstructure evolution during deformation was investigated. It was indicated that the power dissipation efficiency of the composite was relatively lower at higher deformation temperature or lower strain rate. Abnormal grain growth (AGG) and cracking occurred when the composite was deformed at high temperature with low strain rate. A few of CNTs were embedded into coarse grains as AGG occurred, and the micro-cracks formed at the boundaries between the coarse and the fine grained zones. The cracking mechanism was considered as the stress concentration caused by the dragging effect of CNTs, and the reduced critical stress required for pore nucleation due to AGG at the boundaries between the coarse and the fine grained zones.

1. Introduction

Carbon nanotubes (CNTs) have attracted enormous interest globally [1], and are now considered as one of the most potential reinforcements for metal matrix composites due to their remarkable properties including extremely high elastic modulus (~1 TPa) [2] and strength (>30 GPa) [3]. Adding CNTs into aluminum alloys can significantly enhance their strength, thereby broadening their applications, e.g. Liu et al. [4] found the 4.5 vol% CNT/2009Al composite exhibited an ultimate tensile strength of 640 MPa which was 60% higher than that of 2009Al alloy.

As the highest strength aluminum alloys, typical 7xxx Al alloys (i.e. Al–Zn–Mg–Cu) such as 7055Al, 7085Al, etc., are expected to achieve ultra-high strength composites [5]. Wei et al. [6] reported that CNT/7055Al composite exhibited much higher ultimate tensile strength than those of CNT/2xxx Al [7], CNT/5 xxx Al [8], CNT/6xxx Al composites [9]. Therefore, developing CNT/7xxx Al composites and further optimizing processing parameters to manufacture higher performance materials have significant engineering value.

Microstructure evolutions, such as the reinforcement distribution and grain size, are greatly affected by processing parameters. Tavighi et al. [10] found the low temperature deformation could break the reinforcements of Al–16 wt% Al4Sr metal matrix composite, and high temperature deformation promoted the reinforcement non-uniformity distribution. Huang et al. [11] found the dynamic grain growth of SiCp/2014Al composite occurred as the deformation temperature was high, which was the result of dynamic recrystallization (DRX). Ma et al. [12] investigated the hot deformation behavior of SiC/2009Al composite and found that high temperature combined with low strain rate could promote the uniform distribution of the reinforcements. Therefore, processing map is employed to determine processing parameters according to variant deformation behaviors, including DRX, dynamic recovery (DRV) and the flow instability [13]. The processing map investigations of CNT/2xxx Al [14] and CNT/6xxx Al [15] demonstrated that addition of CNTs increased the flow stress, decreased the power dissipation efficiency and broadened unstable domain

* Corresponding author.
** Corresponding author.
E-mail addresses: zyliu@imr.ac.cn (Z.Y. Liu), blxiao@imr.ac.cn (B.L. Xiao).

https://doi.org/10.1016/j.jallcom.2020.157275
0925-8388/

compared to the unreinforced alloys.

The hot deformation behaviors of these CNT/Al composites with varied Al alloy matrixes are quite different. For example, DRX occurred at high temperature with low strain rate in the CNT/2xxx Al composite, which was beneficial to plastic working [14]. However, high temperature with low strain rate induced flow instability in the CNT/6xxx Al composite [15]. Considering that various hot deformation behaviors could be caused by different stacking fault energies [16] and thermal diffusion [17], the CNT/7xxx Al composite might exhibit significantly different hot deformation behaviors from the previous reported CNT/Al composites, as the result of the complicate alloy elements of 7xxx Al alloy matrix.

Furthermore, for materials containing multiple alloy elements, non-uniform grain growth is easy to induce during the sintering process [18]. 7xxx Al alloys have lower melting points due to high alloy content, thus partially melting occurs easily during sintering process. In the CNT/7xxx Al composite with ultra-fine grains formed by ball milling, inhomogeneous grain size might form naturally during the sintering process. Previous studies indicated that the materials with bimodal grain microstructure had quite different deformation behaviors compared to homogeneous materials [19]. For example, the formability of the bimodal magnesium alloy was much weaker than that of the homogeneous magnesium alloy, mainly because the bimodal microstructure was not conducive to uniform plastic deformation [19]. On the other hand, hot deformation also affected the bimodal microstructure evolution. For example, Liu et al. [20] found that hot deformation could promote the grain size homogenization of Udimet 720Li superalloy. That is, the coarse grains were refined due to DRX, while the fine grains were prone to coarsen. In conclusion, for either evaluation of hot working capability or control of the microstructure, it is necessary to study the hot deformation behaviors of CNT/7xxx Al composites. However, to the best of our knowledge, there were no reports focused on hot deformation behaviors of CNT/7xxx Al composites.

In this study, a hot-pressed CNT/7055Al composite was prepared by high energy ball milling combined with powder metallurgy, and the processing maps were established based on hot compression tests. The microstructure evolution and flow instability behavior were analyzed. The aim is to (a) obtain a parameter range suitable for hot working, (b) establish the relationship between processing parameters and microstructure, and (c) clarify the mechanism of micro-crack formation during flow instability.

2. Experimental details

The as-received CNTs had an average length of 5 μm and an average diameter of 15 nm, which was supplied by Tsinghua University. 3.0 vol% CNTs were mechanically mixed with 7055Al (Al-8.1 wt% Zn-2.2 wt% Mg-2.2 wt% Cu) powders in a mixer at a rotation rate of 50 rpm and a ball to powder ratio of 1:1 for 4 h, and then milled in an attritor at a rotation rate of 250 rpm and a ball to powder ratio of 15:1 for 10 h. 2.0 wt % stearic acid was added to prevent severe cold-welding of powders. The as-milled powder was cold-compacted in a cylinder die, degassed, and then hot pressed at 500 °C to a cylindrical billet. The billet was homogenized at 460 °C for 24 h and cooled down to room temperature. For comparison, 7055Al alloy was also fabricated. The fabrication process was similar to that of CNT/7055Al composite.

Cylindrical specimens with a diameter of 8 mm and a height of 12 mm were machined with the axis parallel to the billet axis according to the ASTM E9-09 standard. Isothermal compression tests were conducted at 300, 350, 400, 450 °C and strain rates of 0.001, 0.01, 0.1, 1 s^{-1} using a Gleeble-3800 thermal-simulator system. Graphite sheets were used to lubricate both end surfaces of the specimens. The specimens were rapidly heated to the test temperatures at a heating rate of 10 °C s^{-1} and then held for 10 min to eliminate thermal gradient. The specimens were compressed to a true strain of 0.8 at a constant strain rate, and the true stress-true strain curves were automatically recorded. After hot compression, the specimens were immediately quenched into water to freeze the microstructures. The specimens were cut through the centerline along the compression direction for microstructure examinations.

The specimens were mechanically polished and etched using the Graff and Sargent's reagent, then observed by optical microscopy (OM, Zeiss Axiovert 200 MAT). Microstructures were also examined by scanning electron microscopy (SEM, Quanta 600) and transmission electron microscopy (TEM, FEI Tecnai Spirit TEM T12). TEM specimens were cut by electrical discharge machining, ground to a thickness of 60 μm, then punched to disks with a diameter of 3 mm and then dimpled to a minimum thickness of 20 μm, finally ion-beam thinned by a Gatan Model 691 ion milling system.

The differential scanning calorimetry (DSC, TA-Q1000 system) analysis was carried out using about 10 mg as-milled CNT/7055Al powders. The testing temperature was from 200 °C to 680 °C with a heating rate of 5 °C/min. The density of the CNT/7055Al composite billet was measured using the Archimedes method to evaluate the level of densifications. The oxygen content of the billet was measured with a Leco TC-436 Nitrogen/Oxygen Determinator, and the Fe content was measured with a iCAP Q mass spectrometer.

3. Results and discussion

3.1. Initial microstructure

The measured density of the as hot-pressed CNT/7055Al composite was 2.78 g/cm^3, which reached the theoretical density. The oxygen and Fe content of the composite were respectively 0.34 wt% and 0.11 wt%. It should be mentioned that the impurity of oxidation and Fe was a common phenomenon for milled materials. The microstructures of the as hot-pressed CNT/7055Al composite are shown in Fig. 1. As expected, the hot-pressed CNT/7055Al composite was of dual-scale grain structure (Fig. 1a) without micropore. Through the statistics of the area of different chroma by Image Tool software, the coarse grained zone was accounted for about 15 vol%. Some undissolved phases could be observed in the CNT/7055Al composite, and EDS analysis identified that the undissolved phases were rich in Zn, Mg, and Cu (Fig. 1b). It indicates that the undissolved phase was formed by partial aggregation of alloy elements. TEM images show that the fine grains were equiaxed with an average size of about 200 nm, while the coarse grains exhibited long stripe shape with several microns in the length direction (Fig. 2a). CNTs with a length of 100–200 nm (denoted with black arrows) were uniformly distributed in the fine grained zone without CNT agglomeration, and directionally aligned perpendicular to hot pressing direction, as shown by Fig. 2b. By comparison, almost no CNTs could be observed within the coarse grained zone. It should be mentioned that the inhomogeneous microstructure had not been reported in other previous CNT/Al composites fabricated by conventional powder metallurgy [14].

The presence of the coarse grained zones could be attributed to the formation of liquid phase. Because 7055 Al powders contained large number of alloy elements, such as Zn and Mg, the zones rich in alloy element were prone to melting during hot-pressing. Fig. 3 shows the DSC analysis of the milled 7055Al powders, it can be seen that the powders had an endothermic peak at 486 °C, indicating the melting of the low melting point phase (lower than the hot-pressing temperature of 500 °C). It is believed that the liquid phase was easy to expand to the surfaces of the milled powders. As a result, a larger grain size would be formed at the spaces among Al

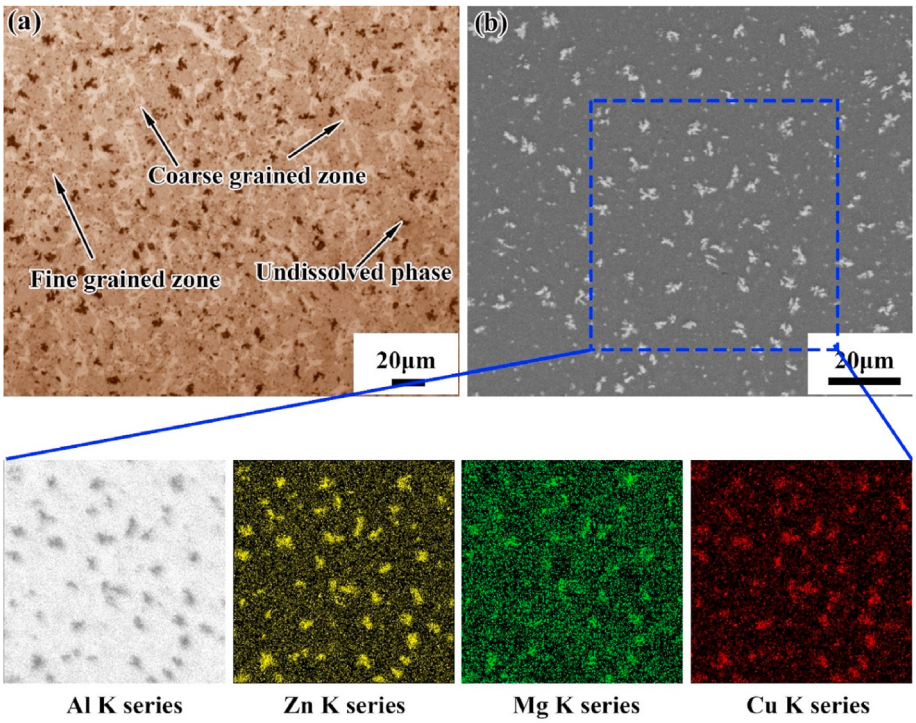

Fig. 1. Microstructure of as hot-pressed 3 vol% CNT/7055Al composite: (a) OM image of macrostructure, (b) SEM back-scattered electron image (Chemical composition of undissolved phases was identified as rich in Zn, Mg and Cu by EDS elemental maps).

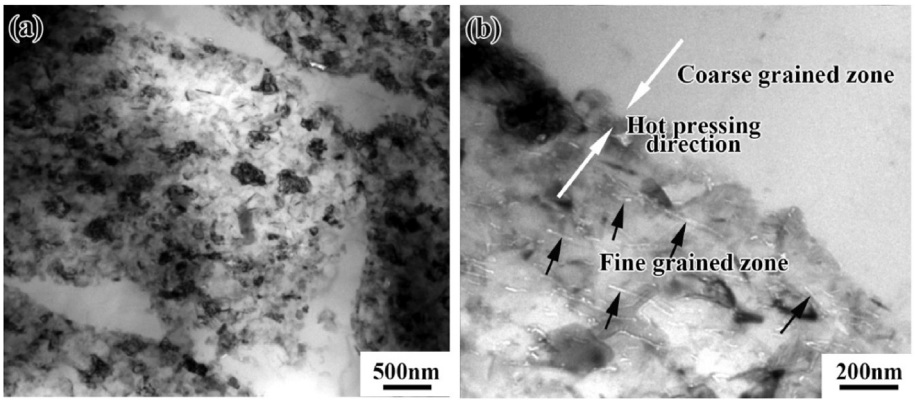

Fig. 2. TEM images of as hot-pressed 3 vol% CNT/7055Al composite: (a) grain microstructure, (b) CNT distribution.

powders after solidification. This is in accordance with previous investigation that the grain size formed by liquid solidification in powder metallurgy route was much large [18]. Furthermore, CNTs were mainly distributed inside the milled powders, and thus CNTs could not move with the liquid during hot-pressing. As a result, no CNTs could be observed inside the coarse grained zones.

3.2. True stress-true strain curves

The typical true stress-true strain curves of the 7055Al alloy and CNT/7055Al composite specimens hot-compressed at 400 °C and strain rate of 0.01 s^{-1} are respectively shown in Fig. 4a and b. It can be seen that flow stress of the matrix alloy and composite decreased as temperature increased or strain rate decreased, and the stress of the composite was higher than that of the matrix alloy. The variation of flow stress with deformation parameters was similar to that of the corresponding CNT/Al composite, but the high stress of the composite indicates that CNTs could still lead to the strengthening effect at high temperature [21].

All the composite specimens hot-compressed to a true strain of 0.8 are shown in Fig. 5. It is readily noted that surface cracks appeared in the specimens deformed at 400 °C with 0.001 s^{-1}, 450 °C with 0.001 s^{-1} and 450 °C with 0.01 s^{-1}. Cracking at higher temperatures with lower strain rates in the present CNT/7055Al composite was not found in previously reported CNT/2xxx Al [21] or CNT/6xxx Al composites [15]. It indicates that the present composite had special hot deformation behaviors.

3.3. Processing maps

The power dissipation efficiency (η) of the 7055Al alloy matrix and CNT/7055Al composite deformed at different parameters were

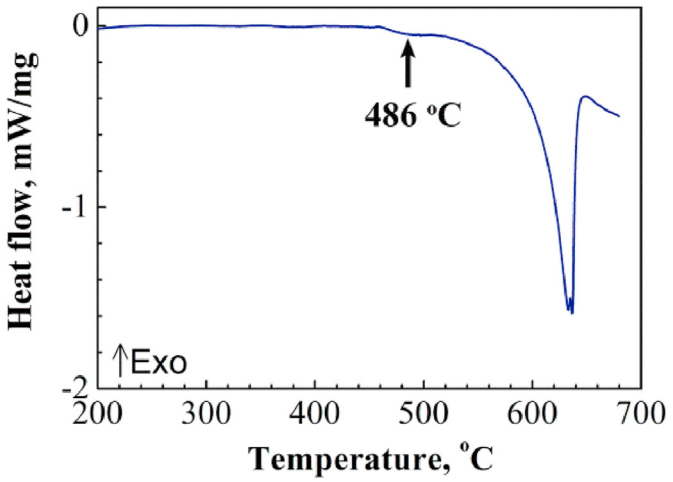

Fig. 3. DSC curves of as-milled CNT/7055Al powders at different temperatures.

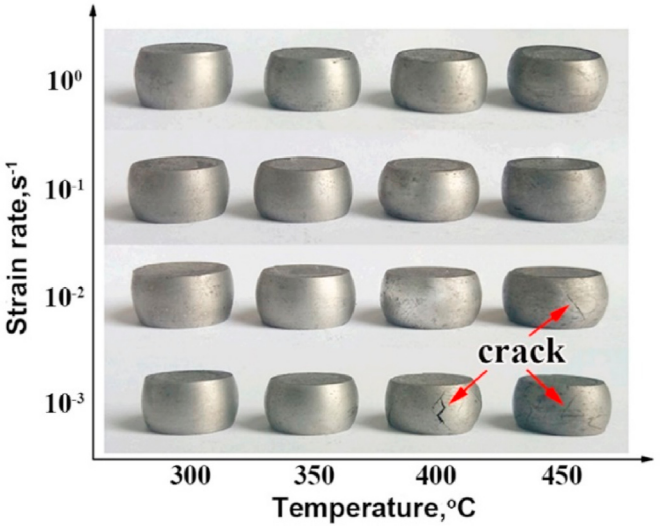

Fig. 5. Morphologies of 3 vol% CNT/7055Al composite specimens hot-compressed to a true strain of 0.8.

both calculated based on Murty model [22]. For the 7055Al alloy matrix, the highest and lowest η of 0.74 and 0.22, were respectively obtained at 420 °C with 1 s^{-1}, and 340 °C with 0.001 s^{-1} (Fig. 6a). The η evolution was similar with that of other reported 7xxx alloy [24], in which DRX was easy to occur at high temperature with high strain rate, and the adequate DRX was good for obtaining a high η.

Unlike the 7xxx Al alloy, the present CNT/7055Al composite exhibited decreased η with increasing temperature from 300 to 400 °C or decreasing strain rate from 1 to 0.001 s^{-1} (Fig. 7a). Especially, as the temperature was higher than 400 °C, η was quite low, even smaller than 0.1. Considering the inhomogeneous microstructure and CNT distribution in present CNT/7055Al composite, the relationship between microstructure evolution and flow behavior must be taken into account for the special variation of η with temperature and strain rate, which will be discussed after microstructure observation.

The instability zones of 7055Al alloy and CNT/7055Al composite were determined using Prasad model [23], as shown by the shaded area in Figs. 6b and 7b. It is apparent that both materials exhibited the instability zones at high temperature with low strain rate. Meanwhile, the processing parameters corresponding to the cracking of CNT/7055Al composite in Fig. 3 were completely covered by the instability zone, which means that the processing maps could well describe the deformation behavior of the CNT/7055Al composite. Furthermore, the range of instability zones in the CNT/7055Al composite was much larger than that of the 7055Al alloy, which indicates that the processing capability of the composite was more difficult than that of the matrix.

3.4. Microstructures evolution

The OM images of the 3 vol% CNT/7055Al composite after hot compression are shown in Fig. 8. A large number of undissolved phases (black particles) could still be observed in the specimens deformed at 300 °C (Fig. 8a and b), while the undissolved phases were much fewer in the specimens deformed at 450 °C (Fig. 8c and d). This indicates that undissolved phases rich in Zn, Mg and Cu could be dissolved during deformation at higher temperatures. The content of coarse grained zones were counted as 16, 14, 16 and 37 vol% for the specimens deformed at 300 °C with 1 s^{-1}, 300 °C with 0.001 s^{-1}, 450 °C with 0.001 s^{-1}, 450 °C with 0.001 s^{-1}, respectively. Obviously, the specimen deformed at 450 °C with 0.001 s^{-1} had a much higher content of coarse grained zones than other specimens (Fig. 8d). This implies that there was an obvious abnormal grain growth (AGG) under this parameter.

Fig. 9 shows the TEM images of the hot-compressed composite specimens. For the specimen deformed at 300 °C with 1 s^{-1} (Fig. 9a and b), a large number of tangled dislocations were observed in the coarse grains. The dislocation density in the fine grained zone was much lower than that in the coarse grained zone. The lower dislocation density within the fine grains might be explained by following reasons. Firstly, the fine grains were more likely to trigger grain boundary (GB) sliding, thereby reducing the number of dislocation nucleation [25]. Secondly, the GB numbers in the fine

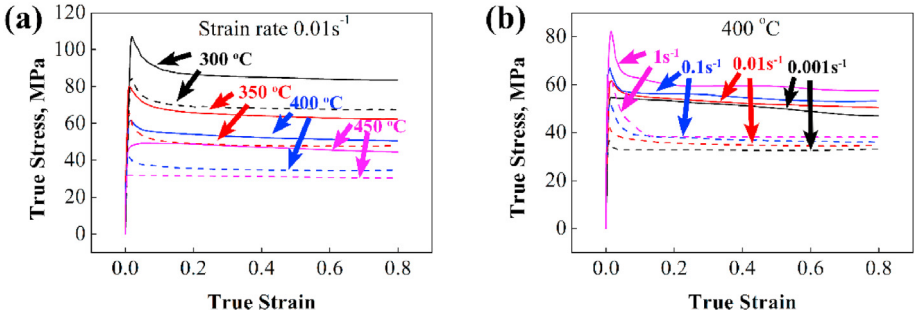

Fig. 4. True stress-true strain curves of 3 vol% CNT/7055Al composite (continuous lines) and 7055Al alloy (dashed lines) specimens hot-compressed at (a) 400 °C and (b) 0.01 s^{-1}.

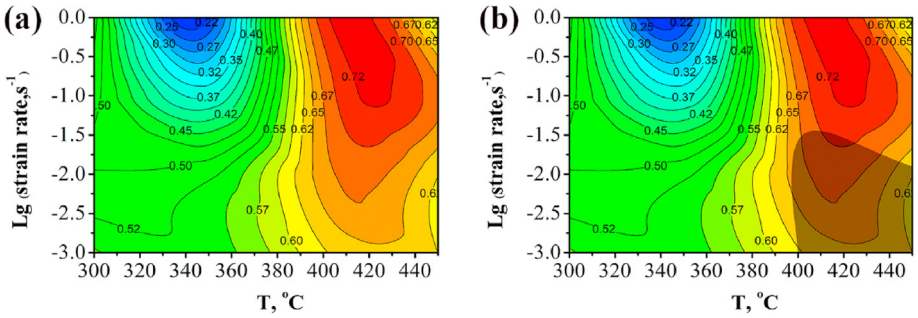

Fig. 6. Processing maps of 7055Al alloy: (a) power dissipation map, (b) processing map containing the unstable zone.

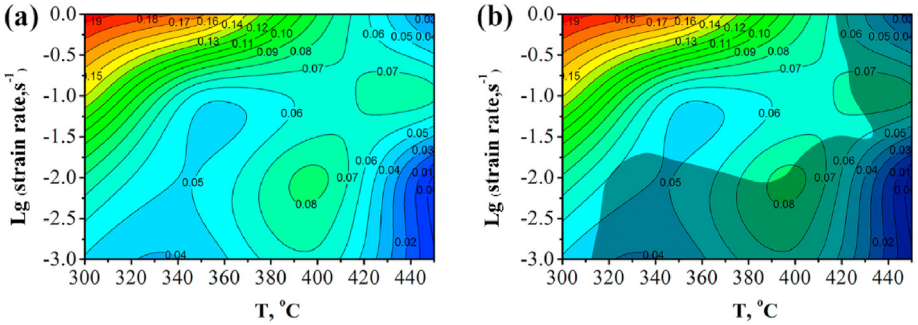

Fig. 7. Processing maps of 3 vol% CNT/7055Al composite: (a) power dissipation map, (b) processing map containing the unstable zone.

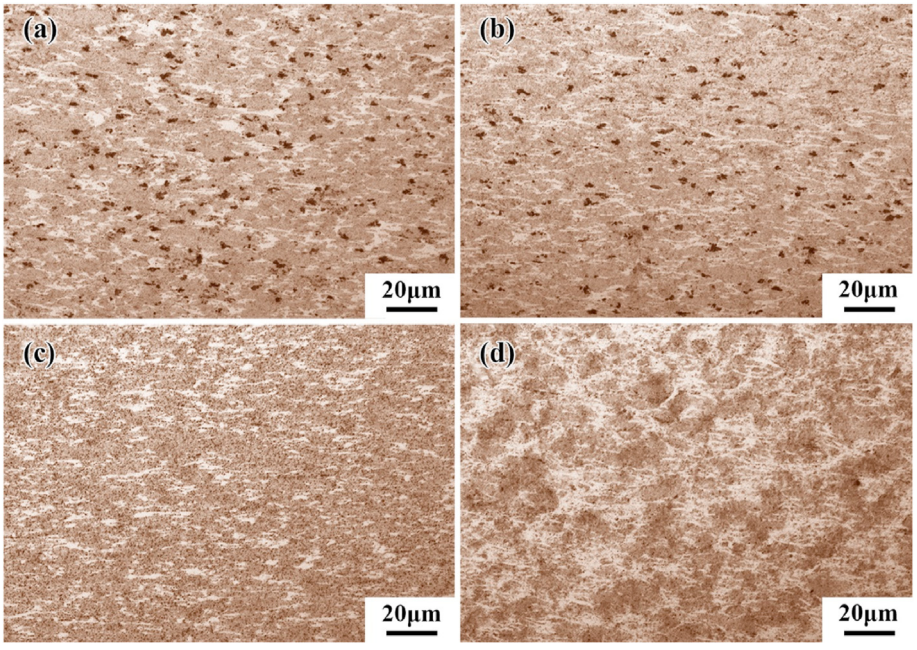

Fig. 8. OM images of CNT/7055Al composite specimens hot-compressed to a true strain of 0.8 at (a) 300 °C with 1s^{-1}, (b) 300 °C with 0.001 s^{-1}, (c) 450 °C with 1 s^{-1} and (d) 450 °C with 0.001 s^{-1}.

grained zone were high, and dislocations could annihilate fast at the GBs [26]. Although fewer dislocations could be observed in the fine grained zone, dislocation walls were found within fine grains, as shown by Fig. 9b. This indicates that DRV occurred within the fine grained zone, and this was another reason for the low dislocation density in the fine grained zone.

According to description of DRV in Ref. [27], opposite sign dislocations attracted each other by climbing or cross-slipping and then disappeared, while the same sign dislocations repelled each other and arranged directionally on the same slip plane to form dislocation walls or sub-grain boundaries. Such dislocation configuration evolution would lead to power dissipation increase [28]. By contrast, dislocations were tangled in the coarse grained zone. This dislocation configuration consumed the imported power

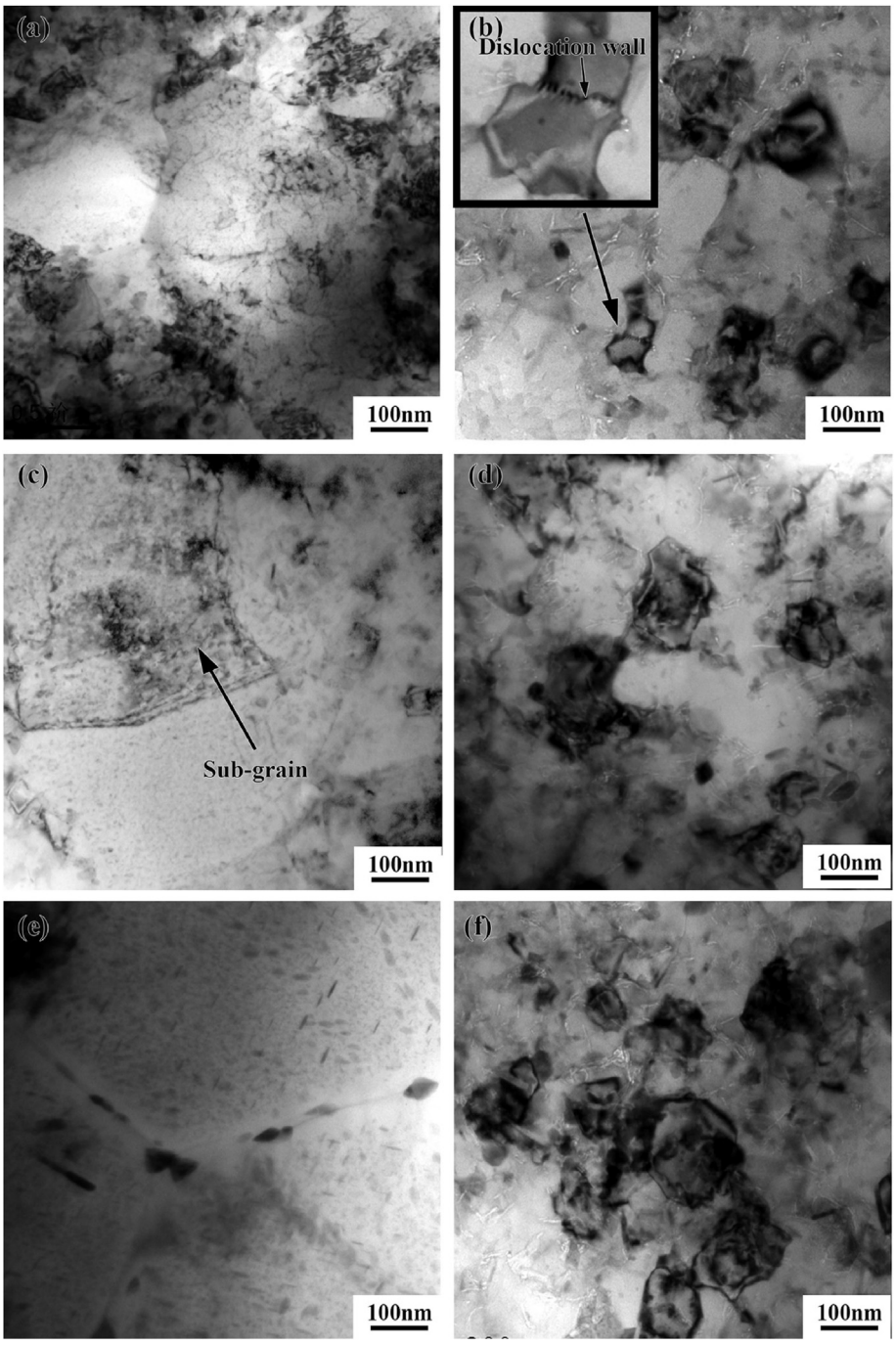

Fig. 9. TEM images of CNT/7055Al composite specimens hot-compressed to a true strain of 0.8 at (a) (b) 300 °C with 1 s^{-1}, (c) (d) 450 °C with 1 s^{-1}, (e) (f) 450 °C with 0.001 s^{-1}.

substantially in the form of heat dissipation. Therefore, the power stored in the microstructure evolution of the coarse grained zone was relatively low. However, as the main part of the composite, the fine grained zone dissipated a large amount of power due to DRV. As a result, the highest η was obtained at 300 °C with 1 s^{-1}.

For the composite specimen deformed at 450 °C with 1 s^{-1} (Fig. 9c and d), the dislocation density in the coarse grains was relatively lower. This could be caused by the GB sliding and the reduced intragranular deformation component due to the high deformation temperature [29]. Further, sub-grains formed within the coarse grains under this deformation parameter. This microstructure agreed well with continuous DRX [30]. By contrast, the substructures such as dislocation walls or sub-grain boundaries were not found in the fine grains.

It should be pointed out that deformation at high temperature with high strain rate was able to induce DRX of 7xxx Al alloy [31], leading to grain refinement accompanied with high η. Unlike the uniform coarse-grained Al alloy, the present CNT/7055Al composite had a high content of fine grains and low content of coarse grains. The fine grain size remained unchanged after hot compression test (Fig. 9d), due to the pinning effect of CNT. Because the fine grain size was far below the lower limited sub-grain size (about 2 μm) of Al alloys at elevated temperatures [32], the fine grains were difficult to further refine by DRX. Furthermore, no DRV evidence was found in

the fine grained zone as mentioned above. As a result, a low η of the composite was obtained under this parameter, although the occurrence of DRX in the coarse grained zone should result in high power dissipation.

For the composite specimen deformed at 450 °C with 0.001 s^{-1}, the content of coarse grained zones increased significantly after hot compression compared to that of the as hot-pressed composite. It can be seen from Fig. 9f that the grain size within the fine grained zone was almost the same as that of the as hot-pressed composite specimen. It has been reported that the grain growth of nanoparticles/metal composites was very difficult due to the strong pinning effect of reinforcements on the GBs [33]. In the present CNT/7055Al composite, the pinning effect of CNTs on the GBs was also confirmed at most of the compression test parameters. Conversely, it could also be ensured that the increased content of the coarse grained zone was not caused by AGG of the fine grains but the coarse grains. That is, the grains in the coarse grained zone preferentially grew along the boundaries into the fine grained zone.

According to the η map (Fig. 6a), it is known that the η corresponding to the AGG was extremely low. This is consistent with the previous study on SiC/2014Al composite [34]. There were mainly two reasons for the low η. On one hand, the content of the GBs reduced and the GB energy decreased due to AGG, so the power stored in the GBs decreased. On the other hand, AGG aggravated the inhomogeneous microstructure, and easily led to localized deformation. Because the effective area for power dissipation was reduced, and thus the extremely low η was obtained.

Fig. 10 shows the TEM images of the composite specimens hot-compressed at 300 °C with 1 s^{-1} (without AGG) and 450 °C with 0.001 s^{-1} (with AGG). It can be seen CNTs maintained good structure morphology. According to the previous characterization results of the CNTs in the CNT/Al composite after hot extrusion [8], it can be known that the common hot deformation would not lead to severe damage of CNTs. However, the distribution of CNTs would be changed with different deformation parameters. Compared to the as hot-pressed composite specimen (Fig. 2b), the orientation of CNTs in both composite specimens became chaotic after hot compression. This is mainly attributed to CNT rotation driven by the matrix alloy flow during hot deformation. No CNTs were observed in the coarse grains after hot deformation at 300 °C with 1 s^{-1} (Fig. 10a), while some CNTs were embedded into the coarse grained zone after hot deformation at 450 °C with 0.001 s^{-1}.

It is believed that the boundaries between the coarse and the fine grained zones broke through the pinning effect of CNTs and migrated from the coarse grained zone to the fine grained zone during hot deformation at 450 °C with 0.001 s^{-1}. This result is in accordance with the previous finding [35] that the externally applied stress during hot deformation could assist the GB migration to break through the pinning effect of the reinforcements and promote grain growth. Overall, for the CNT/7055Al composite with initial inhomogeneous microstructure, the boundaries between the coarse and the fine grained zones were unstable under external stress due to stress concentration, thereby resulting in preferential GB migration at these positions, and the AGG phenomenon appeared as a result.

3.5. Cracking mechanism analysis

In previous investigations on hot deformation of Al alloy [31] or particle reinforced Al matrix composite [34], GB sliding and atomic diffusion were confirmed during deformation at high temperature with low strain rate, thereby reducing the risk of cracking. However, for the CNT/7055Al composite, the external cracks were observed in the composite specimens deformed at high temperature with low strain rate (Fig. 5). This could be related to AGG and the dragging effect of CNTs on the GBs.

The dragging effect of reinforcements can be expressed by the following equation [36].

$$\tau = \eta_I \frac{dv}{dh} \tag{1}$$

where τ is the dragging force, v is the deformation velocity of the viscous layer, h is the thickness of the viscous layer, and η_I is the interface viscosity, which can be expressed by the following equation [37].

$$\eta_I = \frac{kT}{8bD} \tag{2}$$

where k is the constant, T is temperature, b is the atom spacing, D is the diffusion coefficient. Substituting Eq. (2) into Eq. (1), the final form of Eq. (1) can be changed to

$$\tau = \frac{kT}{8bD}\frac{dv}{dh} \tag{3}$$

Eq. (3) demonstrates that the increase of temperature could produce a higher dragging force. When GB sliding in the CNT/Al composites was triggered during deformation, the enhanced dragging effect of CNTs could aggravate the stress concentration at

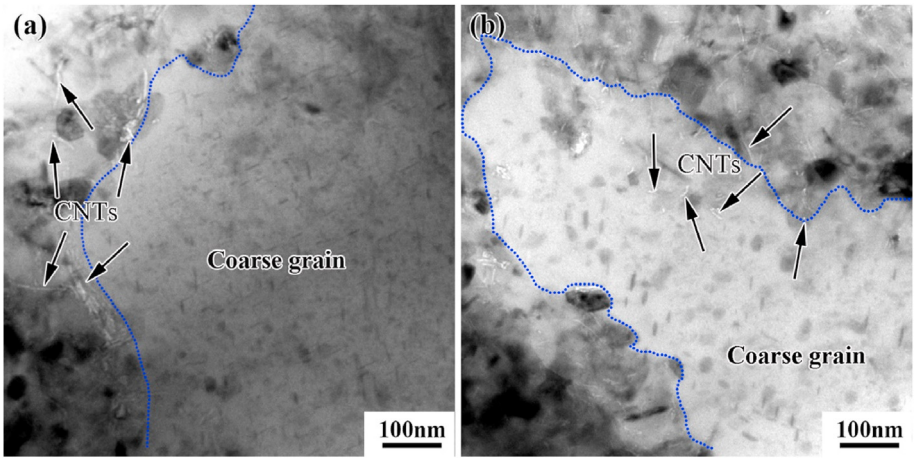

Fig. 10. TEM images of the composite specimens hot-compressed to a true strain of 0.8 at (a) 300 °C with 1 s^{-1} and (b) 450 °C with 0.001 s^{-1}.

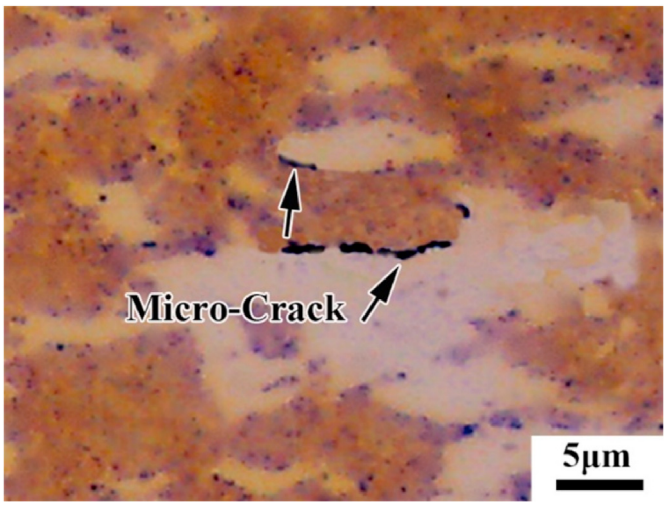

Fig. 11. Micro-crack initiation in CNT/7055Al composite hot-compressed at 450 °C with 0.001 s^{-1}.

the GBs, thereby increasing the risk of damage. On the other hand, the stress concentration at the GBs is also related to the grain size. Smith et al. [38] deduced that the stress required for nucleation of the pores at the second phase particles could be expressed by

$$\tau_{\infty} = \left[\frac{\pi\gamma_s E}{(1-\nu^2)P}\right]^{1/2}\left(\frac{P}{\lambda}\right) \quad (4)$$

where τ_{∞} is the shear stress required for the nucleation of the pores, γ_s is the surface energy of the pores, E is the Young's modulus of the matrix, ν is the Poisson's ratio of the matrix, P is the diameter of the second phase particles, and λ is the sub-grain size. Eq. (4) indicates that the increase of subgrain or grain size could decrease the required stress of cracking. It means that AGG would increase the risk for cracking.

Fig. 11 shows the micro-crack in the composite hot-compressed at 450 °C with 0.001 s^{-1}. It can be seen that the micro-cracks with width less than 1 μm were located at the boundaries between the coarse and the fine grained zones, and almost no micro-cracks can be observed in the neighborhood of the coarse grained zones.

The schematic of cracking during deformation is drawn in Fig. 12. For the as hot-pressed composite, the grains were inhomogenous, composed of coarse grains and fine grains with some CNTs distributed at the GBs. During hot deformation at high temperature with low strain rate, GB sliding became easy, which led to stress concentration at the boundaries between the coarse and the fine grained zones due to dragging effect of CNTs. On the other hand, stress concentration was aggravated and the critical stress required for pore nucleation reduced due to AGG. As a result, micro-cracks would form at the boundaries between the coarse and the fine grained zones.

4. Conclusions

In this study, hot compression test was employed to investigate the hot deformation behavior of the 3.0 vol% CNT/7055Al composite at temperatures ranging from 300 to 450 °C with strain rates ranging from 0.001 to 1 s^{-1}. The following conclusions can be drawn:

(1) The as hot-pressed composite had an inhomogeneous microstructure composed of CNT-free coarse grains and fine grains with uniformly dispersed CNTs. There were some undissolved phases rich in Zn, Mg, and Cu in the as hot-pressed composite, and the undissolved phases were greatly reduced after the composite was deformed at high temperature (450 °C).
(2) The power dissipation efficiency was decreased as the temperature increased or the strain rate decreased. The lowest

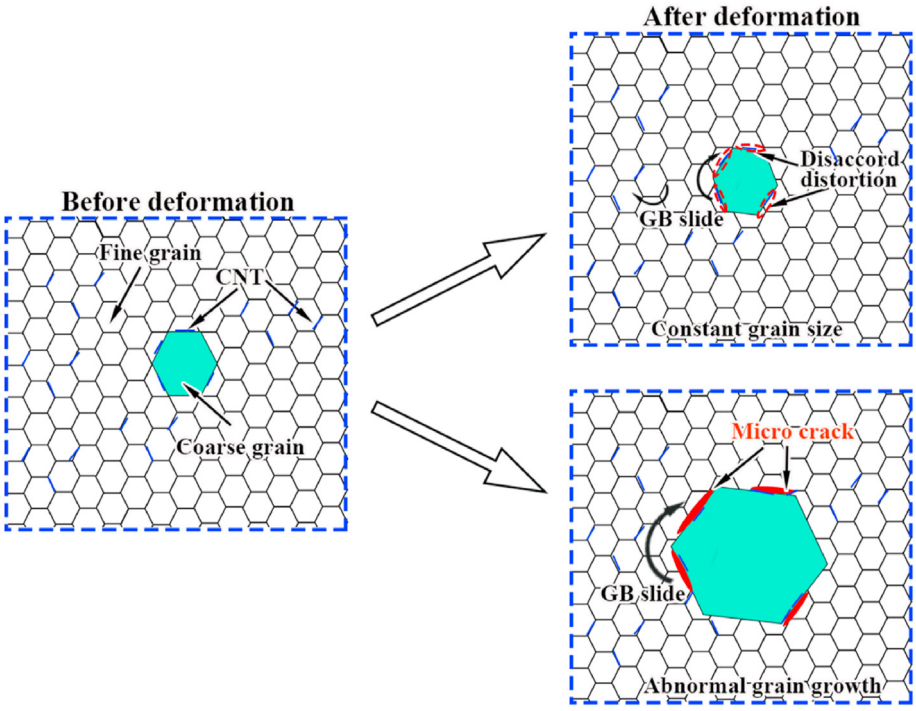

Fig. 12. Cracking schematic of CNT/7055Al composite (AGG occurred as the composite deformed at high temperature with low strain rate).

power dissipation efficiency was only 0.01 at 450 °C with 0.001 s^{-1}, due to the decrease of energy stored at the GBs and the severe localized deformation induced by AGG.

(3) AGG was observed for the composite deformed at high temperature with low strain rate, and some CNTs were embedded into the coarse grains as AGG occurred. It is believed that the boundaries between the coarse and the fine grained zones broke through the pinning effect of CNTs, and migrated from the coarse grained zone to the fine grained zone, thereby forming the AGG.

(4) The cracking occurred as the composite was deformed at high temperature with low strain rate, and micro-cracks mainly formed at the boundaries between the coarse and the fine grained zones. This was attributed to the stress concentration induced by the dragging effect of CNTs, and the reduced critical stress required for pore nucleation due to AGG at the boundaries between the coarse and the fine grained zones.

CRediT authorship contribution statement

K. Ma: Data curation, Formal analysis, carried out the data collection, data analysis and manuscript writing; All authors contribute substantially to the paper. All authors read and approved the final manuscript. **Z.Y. Liu:** fabricated the composites, revised the manuscript and provided the fund; Ma revised the manuscript and provided the fund. All authors read and approved the final manuscript. All authors contribute substantially to the paper. All authors read and approved the final manuscript. **X.X. Zhang:** Formal analysis, helped to analyze the microstructure; All authors contribute substantially to the paper. All authors read and approved the final manuscript. **B.L. Xiao:** designed the experiment and provided the fund; All authors read and approved the final manuscript. **Z.Y. Ma:** revised the manuscript and provided the fund. All authors read and approved the final manuscript. All authors contribute substantially to the paper.

Declaration of competing interest

The authors declare that they have no known competing financial interests or personal relationships that could have appeared to influence the work reported in this paper.

Acknowledgments

This work was supported by: (a) Key Research Program of Frontier Sciences, CAS (No. QYZDJ-SSW-JSC015); National Key R&D Program of China (No. 2017YFB0703104); (b) National Natural Science Foundation of China (No. 51931009, No.51871214, No. 51871215); (c) the Youth Innovation Promotion Association CAS (2020197), (d) Guangxi Natural Science Foundation (No. 2016GXNSFDA380028).

References

[1] Z.Y. Liu, K. Ma, G.H. Fan, K. Zhao, J.F. Zhang, B.L. Xiao, Z.Y. Ma, Enhancement of the strength-ductility relationship for carbon nanotube/Al-Cu-Mg nanocomposites by material parameter optimisation, Carbon 157 (2020) 602–613.
[2] S.C. Tjong, Recent progress in the development and properties of novel metal matrix nanocomposites reinforced with carbon nanotubes and graphene nanosheets, Mater. Sci. Eng. R 74 (2013) 281–350.
[3] K. Zhao, Z.Y. Liu, B.L. Xiao, D.R. Ni, Z.Y. Ma, Origin of insignificant strengthening effect of CNTs in T6-treated CNT/6061Al composites, Acta Metall. Sin. 31 (2018) 134–142.
[4] Z.Y. Liu, B.L. Xiao, W.G. Wang, Z.Y. Ma, Developing high-performance aluminum matrix composites with directionally aligned carbon nanotubes by combining friction stir processing and subsequent rolling, Carbon 62 (2013) 35–42.
[5] J.C. Williams, E.A. Starke, Progress in structural materials for aerospace systems11The golden jubilee issue—selected topics in materials science and engineering: past, present and future, in: S. Suresh (Ed.), Acta Mater vol. 51, 2003, pp. 5775–5799.
[6] H. Wei, Z. Li, D.B. Xiong, Z. Tan, G. Fan, Z. Qin, D. Zhang, Towards strong and stiff carbon nanotube-reinforced high-strength aluminum alloy composites through a microlaminated architecture design, Scripta Mater. 75 (2014) 30–33.
[7] H.J. Choi, B.H. Min, J.H. Shin, D.H. Bae, Strengthening in nanostructured 2024 aluminum alloy and its composites containing carbon nanotubes, Composites Part A 42 (2011) 1438–1444.
[8] Z.Y. Liu, B.L. Xiao, W.G. Wang, Z.Y. Ma, Modelling of carbon nanotube dispersion and strengthening mechanisms in Al matrix composites prepared by high energy ball milling-powder metallurgy method, Composites Part A 94 (2017) 189–198.
[9] M. Chen, G. Fan, Z. Tan, C. Yuan, Q. Guo, D. Xiong, M. Chen, Q. Zheng, Z. Li, D. Zhang, Heat treatment behavior and strengthening mechanisms of CNT/6061Al composites fabricated by flake powder metallurgy, Mater. Char. 153 (2019) 261–270.
[10] K. Tavighi, M. Emamy, A.R. Emami, Effects of extrusion temperature on the microstructure and tensile properties of Al-16 wt% Al_4Sr metal matrix composite, Mater. Des. 46 (2013) 598–604.
[11] Z.Y. Huang, X.X. Zhang, C. Yang, B.L. Xiao, Z.Y. Ma, Abnormal deformation behavior and particle distribution during hot compression of fine-grained 14vol% SiCp/2014Al composite, J. Alloys Compd. 743 (2018) 87–98.
[12] K. Ma, X.X. Zhang, D. Wang, Q.Z. Wang, Z.Y. Liu, B.L. Xiao, Z.Y. Ma, Optimization and simulation of deformation parameters of SiC/2009Al composites, Acta Metall. Sin. 55 (2019) 1329–1337.
[13] Y. Prasad, H.L. Gegel, S.M. Doraivelu, J.C. Malas, J.T. Morgan, K.A. Lark, D.R. Barker, Modeling OF dynamic material behavior IN hot deformation - forging OF TI-6242, Metall. Trans. A 15 (1984) 1883–1892.
[14] F. Mokdad, D.L. Chen, Z.Y. Liu, D.R. Ni, B.L. Xiao, Z.Y. Ma, Three-dimensional processing maps and microstructural evolution of a CNT-reinforced Al-Cu-Mg nanocomposite, Mater. Sci. Eng., A 702 (2017) 425–437.
[15] W.J. He, C.H. Li, B.F. Luan, R.S. Qiu, K. Wang, Z.Q. Li, Q. Liu, Deformation behaviors and processing maps of CNTs/Al alloy composite fabricated by flake powder metallurgy, Trans. Nonferrous Metals Soc. China 25 (2015) 3578–3584.
[16] S. Wang, J.R. Luo, L.G. Hou, J.S. Zhang, L.Z. Zhuang, Physically based constitutive analysis and microstructural evolution of AA7050 aluminum alloy during hot compression, Mater. Des. 107 (2016) 277–289.
[17] H. Huang, G. Fan, Z. Tan, D.-B. Xiong, Q. Guo, C. Guo, Z. Li, D. Zhang, Superplastic behavior of carbon nanotube reinforced aluminum composites fabricated by flake powder metallurgy, Mater. Sci. Eng., A 699 (2017) 55–61.
[18] R.M. German, Coarsening in sintering: grain shape distribution, grain size distribution, and grain growth kinetics in solid-pore systems, Crit. Rev. Solid State Mater. Sci. 35 (2010) 263–305.
[19] J.A. del Valle, O.A. Ruano, Superplasticity in a magnesium alloy prepared with bimodal grain size distributions developed by dynamic recrystallisation, Mater. Lett. 62 (2008) 3391–3394.
[20] F. Liu, J. Chen, J. Dong, M. Zhang, Z. Yao, The hot deformation behaviors of coarse, fine and mixed grain for Udimet 720Li superalloy, Mater. Sci. Eng., A 651 (2016) 102–115.
[21] C.H. Li, R.S. Qiu, B.F. Luan, W.J. He, Z.Q. Li, Hot deformation and processing maps of as-sintered CNT/Al-Cu composites fabricated by flake powder metallurgy, Trans. Nonferrous Metals Soc. China 28 (2018) 1695–1704.
[22] S. Murty, B.N. Rao, Instability map for hot working of 6061 Al-10 vol% Al2O3 metal matrix composite, J. Phys. D Appl. Phys. 31 (1998) 3306–3311.
[23] Y. Prasad, Recent advances IN the science OF mechanical processing, Indian J. Technol. 28 (1990) 435–451.
[24] D. Xiao, X. Peng, X. Liang, Y. Deng, G. Xu, Z. Yin, Study on hot workability of Al-5.87Zn-2.07Mg-2.28Cu alloy using processing map, J. Occup. Med. 69 (2017) 725–733.
[25] J.W. Edington, K.N. Melton, C.P. Cutler, Superplasticity, Prog. Mater Sci. 21 (1976) 61–170.
[26] N. Ahmed, A. Hartmaier, Mechanisms of grain boundary softening and strain-rate sensitivity in deformation of ultrafine-grained metals at high temperatures, Acta Mater. 59 (2011) 4323–4334.
[27] Y. Deng, Z. Yin, J. Huang, Hot deformation behavior and microstructural evolution of homogenized 7050 aluminum alloy during compression at elevated temperature, Mater. Sci. Eng., A 528 (2011) 1780–1786.
[28] K. Schulz, D. Dickel, S. Schmitt, S. Sandfeld, D. Weygand, P. Gumbsch, Analysis of dislocation pile-ups using a dislocation-based continuum theory, Model. Simulat. Mater. Sci. Eng. 22 (2014).
[29] Y.Q. Wu, H.J. Shi, K.S. Zhang, H.Y. Yeh, Numerical investigation of grain boundary effects on elevated-temperature deformation and fracture, Int. J. Solid Struct. 43 (2006) 4546–4577.
[30] B.L. Xiao, Z.Y. Huang, K. Ma, X.X. Zhang, Z.Y. Ma, Research on hot deformation behaviors of discontinuously reinforced aluminum composites, Acta Metall. Sin. 55 (2019) 59–72.
[31] Y.C. Lin, L.T. Li, Y.C. Xia, Y.Q. Jiang, Hot deformation and processing map of a typical Al–Zn–Mg–Cu alloy, J. Alloys Compd. 550 (2013) 438–445.
[32] A. Gholinia, F.J. Humphreys, P.B. Prangnell, Production of ultra-fine grain

microstructures in Al–Mg alloys by coventional rolling, Acta Mater. 50 (2002) 4461–4476.
[33] A. Esawi, K. Morsi, Dispersion of carbon nanotubes (CNTs) in aluminum powder, Composites Part A 38 (2007) 646–650.
[34] Z. Huang, X. Zhang, B. Xiao, Z. Ma, Hot deformation mechanisms and microstructure evolution of SiCp/2014Al composite, J. Alloys Compd. 722 (2017) 145–157.
[35] Y. Lin, H. Wen, Y. Li, B. Wen, W. Liu, E.J. Lavernia, An analytical model for stress-induced grain growth in the presence of both second-phase particles and solute segregation at grain boundaries, Acta Mater. 82 (2015) 304–315.
[36] T.G. Nieh, J. Wadsworth, T. Imai, A rheological view of high-strain-rate superplasticity in alloys and metal-matrix composites, Scripta Mater. 26 (1992) 703–708.
[37] M.F. Ashby, Boundary defects, and atomistic aspects of boundary sliding and diffusional creep, Surf. Sci. 31 (1972) 498–542.
[38] E. Smith, J.T. Barnby, Nucleation of grain-boundary cavities during high-temperature creep, Metal Science Journal 1 (1967) 1–4.